RESEARCH PAPER

Soft Computing Based Parametric Optimization of Cutting Rate, Surface Roughness, and Kerf Width in Wire Electric Discharge Machining of High Strength Ti-3Al-2.5 V

Anshuman Kumar[1] · Chandramani Upadhyay[2] · Naveen Kumar[3] · A. V. S. Ram Prasad[4] · Dusanapudi Siva Nagaraju[1]

Abstract

The present study focused on the machinability of Ti-3Al-2.5 V for wire-electrical discharge machining (WEDM) using "BroncoCut-X wire" (zinc-coated copper wire). The machining characteristics have been evaluated by varying wire-tension (T_w), wire-speed (S_w), flushing-pressure (P_f), discharge current (I_d), and spark-on-time (S_{on}). The response characteristics associated with cutting-speed (Cs), kerf-width (KW), and surface roughness (RA) have been collected and analyzed using main-effect plots, scanning electron microscope (SEM), and analysis of variance (ANOVA). The maximum Cs and minimum KW and RA are obtained upto 8.90 mm/min, 3.34 μm and 0.2218 mm, respectively. Additionally, the novelty lies in the smart hybrid prediction tool considering the conflicting nature of responses are converted into single responses using Grey Relation Analysis (GRA) and Fuzzy Interference System (FIS) (Namely: Gray-Fuzzy Reasoning Grade (GFRG)). Furthermore, the optimal performance is calculated using Rao-algorithms (i.e., Rao1, Rao2, and Rao3). The obtained ideal machining condition is 16N wire-tension, 3 m/min wire-speed, 8 kg/mm² flushing-pressure, 21A discharge current, and 14 μs spark-on-time. The result has also been compared with the JAYA-algorithm and improved-grey wolf optimizer (I-GWO) to demonstrate the efficacy of the intended approach. The confirmation test has been conducted and obtained that the GFRG-based results are further improved by using a hybrid GFRG-based Rao-algorithm of 9.55%, 2.36%, and 7.99% as Cs, KW and RA, respectively. Furthermore, this study shows that the proposed multi-objective optimization method not only leads to more stable solutions but also to shorter run times and enhanced quality to support engineers in reducing the cost of item failures.

Keywords WEDM · Grey relation analysis · Fuzzy · Rao-Algorithm · JAYA · I-GWO · Hybrid optimization

Introduction

Industrial growth is indeed critical for a country's economy. But, it has a negative impact on the environment in terms of material wastage. Cost-conscious production is a serious concern that runs the industry from normal to sustainable manufacturing. Industrial actors, research institutions, and academic institutions were all compelled to devise new strategies for reducing environmental damage caused by energy and material wastage. Titanium and its alloys are one of important industrial materials where lots of effort and energy are consumed to obtain the required shape. This resulted in the end product of these alloys coming with a lot of industrial wastage.

Titanium and its titanium alloys have vast applications in marine, aerospace, chemical, and as well as biomedical fields. These materials have outstanding properties, which include a high strength-to-weight ratio, the capacity to maintain hardness at high temperatures, significant biocompatibility, and high corrosion and wear resistance.

Among all Ti-alloys, the Ti 3Al-2.5 V (Grade-9 alloy) offers work in both hot and cold environments. This property is ideal for hydraulics machinery that has been set in extremely cold temperatures or subjected to extreme

✉ Anshuman Kumar
  anshu.mit06@gmail.com

1   Department of Mechanical Engineering, Gokaraju Rangaraju Institute of Engineering and Technology, Hyderabad, India

2   Department of Mechanical Engineering, National Institute of Technology Rourkela, Rourkela, India

3   Amity Institute of Information Technology, Amity University, Patna, India

4   Department of Mechanical Engineering, Koneru Lakshmaiah Education Foundation, Vaddeswaram, India

temperatures in hot environments. That is why it is also suitable for aerospace industries, where many moving parts glide through the air in an extremely cold environment. It is also used in the medical and chemical processing sectors for their equipment and machinery because of its capacity to maintain hardness at high temperatures. Furthermore, this alloy belongs to the alpha–beta Ti-alloy, which offers much more strength than other Ti-alloys. The primary application of this alloy nowadays is in fabricating medical and dental implants and high-pressure piping in the hydrogen pumping system of the space shuttle, and it is also used in sports equipment [1]. Many researchers are interested in this alloy because of its expanding use in high-temperature applications.

Producing tight tolerance parts with high quality productivity becomes a challenging task. Tool deformation and excessive tool wear happened due to the strength and hot hardness of the material. The generation of high cutting temperatures and the built-up edge on the cutting tool may emerge during the traditional machining of Ti-alloys. Therefore, selecting a proper tool geometry for the machine is the most important task, and it incurs additional production costs. Therefore, the traditional machining process is inadequate for these "difficult-to-cut" alloys. Owing to this issue, this material is difficult to machine through traditional methods. So, non-traditional machining techniques are being used to obtain the reasonable geometry and surface quality of the end product. But, low Cs must be compromised during non-traditional machining. Among the various non-conventional machining processes, WEDM is the most appropriate and widely accepted non-traditional machining method regarding dimensional accuracy and complex profiling.

WEDM is a thermal-electrical machining process with a continuous travelling wire (electrode) through the workpart. It can machine any electrically conductive material with a different hardness. The end product from this machining process has vast applications in the automobile and aerospace industries due to its better dimension accuracy and shallow material wastage. The characteristics of WEDM may be identified in terms of intricate shapes and precision surface quality. These machining characteristics may be ideal for manufacturing extrusion or stamping dies, prototype components, etc. On the other hand, like every machining process, WEDM is associated with certain limitations or challenges regarding the dimensional accuracy of WEDMed components, which in terms of overcut or undercut, kerf width, dimensional deviation, etc.

State of the Art

Previous researchers have conducted an extensive study using WEDM in an effort to increase profile accuracy while maintaining acceptable dimensional tolerances. Mahapatra et al. [2] developed a methodology to achieve modified machined surfaces while also maintaining accuracy in the WEDM using Taguchi's philosophy. Puri et al. [3] investigated geometrical inaccuracy using the Taguchi method with thirteen process parameters. As a result, wire lag affects average Cs, geometrical inaccuracy, and surface finish characteristics during the investigation. Hariharan et al. [4] identified the best possible method to achieve the KW and surface roughness of Al6351–SiC-based composite using WEDM. The investigators concluded that the current and pulse-on-time both have an impact on the kerf width, but the wire feed rate has a greater impact on the surface roughness.

The WEDM method has been used in several studies on Ti-6Al-4 V (Grade 5) alloy to help minimize roughness and increase MRR performance. This might be because Ti-6Al-4 V is less expensive and easier to manufacture than Ti-3Al-2.5 V. Several papers on Ti-6Al-4 V machining and machinability are listed below. The results of the previous study on Ti-6Al-4 V may assist in understanding the machining responses of Ti-3Al-2.5 V. However, both alloys are under the Ti-alloys and the alpha–beta-Ti alloy category. Shajan and Shunmugam [5] analyzed the issues of the metallurgical changes on Ti-6Al-4 V as a workpart. L_{18} OA has been considered for conducting experiment runs using zinc-coated brass wire (ZnWE) of 0.25 mm diameter. The authors identified pulse-on, T_w, and S_w as the most influential process parameters. Pasam et al. [6] observed that the lower pulse-on time and current result in a good surface finish using ZnWE. Devarajaiah [7] discussed the impacts of machining parameters on MRR and power consumption were explored, and a regression model was also built. The results showed that the model accuracy was 98.34% and 94.03%, respectively, for both machining outcomes. Gupta et al. [8] showed annealing Ti-6Al-4 V to enhance cutting speed and surface quality. This material was machined at a maximum speed of 1.75 m/min using WEDM. Wire tension and servo voltage were the two factors that have been the greatest impact on cutting speed. Sharma et al. [9] proposed a grey and harmony search coupled hybrid optimization method for WEDM parameters to identify the MRR and R_z values of Ti-6Al-4 V biomedical alloy.

The above section discusses various aspects of Ti-6Al-4 V machining using WEDM. Only a few research groups have attempted to analyze the material behaviour under different mechanical and thermal conditions and rare on machining responses of Ti-3Al-2.5 V. Wang et al. [10] investigate a suitable for subsequent measurement and avoid stress relief during EDM process of Ti-3Al-2.5 V tubing. Miller et al. [11] analyze the heat treatment on Ti-3Al-2.5 V to find their mechanical properties. Additionally, the authors conclude that results from the heat treatment processes found that Ti-3Al-2.5 V achieved better mechanical properties, and it may replace with Ti-6Al-4 V. Babu et al. [12] studied the

mechanical and sliding wear characteristics of Ti-3Al-2.5 V using RSM methodology. The authors found that at 90N load, cracks, ploughing, and delamination formed because of high-temperature generation using a "pin on disc" tribometer. Singh et al. [13] identify the sustainable machining and advanced cooling technology of Ti-3Al-2.5 V on turning operation using the coated tool. Babu et al. [14] used Taguchi's based Grey analysis to obtain the best possible machining parameter on Ti-3Al-2.5 V using WEDM. Authors found that wire feed and S_{on} are significantly affected parameters.

The low Cs is a major issue in the WEDM process. It is the primary reason for not achieving high productivity. As a result, only selected WEDMed end products are used in the aerospace industry because of this drawback [15]. On the other hand, the advancements in wire electrodes are going in the research community to increase the Cs, and decrease power consumption and material wastage. The different types of coated and uncoated materials with the different types of core materials are being used to overcome this issue. These wire electrodes are primarily used for high Cs, superior surface finish, and tight machining dimensional accuracy [16, 17]. Selecting a suitable wire electrode are also important for increasing the Cs, and decreasing power consumption and material wastage. Among these characteristics of the wire, Zinc-coated and uncoated wires are basically used for high-performance machining. Meanwhile, the wire electrode cost contributes only 10% to its overall machining cost, so it seems to be very economical to evaluate the wire properties used for optimizing the overall performance of the process [18]. Prohaszka et al. [18] investigated the properties of the wire electrode, which helped to improve the quality of the end product using WEDM. Rehman et al. [16] studied the improvement of higher productivity. The authors found 14.02% and 19.24% improvements in MRR and RA using gamma phase-coated wire on DC53 steel. The comparison of zinc-coated copper wire and uncoated brass wire on Inconel 718 was studied by Reolon et al. [19]. According to the studies, in comparison to the uncoated brass wire, zinc-coated copper wire provides a surface that has a higher level of integrity for the WEDMed Inconel alloy. The above literature shows that coated wires have shown their effectiveness in improving the Cs and reducing wire deflection in the case of the uncoated electrode.

In this pandemic of COVID-19, almost every manufacturing industry is considering suitable and sustainable techniques to obtain favourable machine settings using soft computing where less human gathering and maintain a satisfactory equilibrium between productivity and quality. This means that the rate of production should not be slowed down and not compromised with respect to various quality attributes such as surface quality, dimensional tolerances, etc., and vice versa in terms of time. Implementing an optimization strategy may save production time and cost and give the best

solution to the existing problem. Also, it can be applied to develop or design a new product [20]. Optimizing is a system that involves maximizing or minimizing the value of an objective function and determining which machine settings may produce the best results based on the available sample space [21–23].

The literature review reveals that no works (as per the authors' best knowledge) are attempted to explore the machining behaviour of Ti-3Al-2.5 V with an increase in the cutting speed in the WEDM context. Moreover, identifying the favourable machining parameter settings for obtaining the anticipated performance using hybrid multi-optimization approaches is still untouched. The main contribution of the presented work is to search for a controlled experimental condition for Ti-3Al-2.5 V. A novel soft computing based hybrid optimization strategy (GRA-Fuzzy based Rao-algorithm) has been used to improve the machining outcome (in terms of Cs, KW and RA). Moreover, the impact of wire electrode on the machining characteristics (especially cutting speed and surface integrity) has been assessed using "BroncoCut-X" wire. The effect of said electrode on microstructural aspects such as craters, re-solidified debris, spherical droplets and cracks has also investigated.

Experimentation

The experimental runs are carried out on a Ti-3Al-2.5 V plate ($40 \times 30 \times 5\ mm^3$). Figure 1 depicts a schematic diagram of the machined profile. Figure 2 displays the EDS elemental spectra of the workpiece utilized in this study. These spectra indicate the chemical composition of the workpiece as received. Table 1 shows the salient properties of Ti-3Al-2.5 V. Experimentation has been performed on the "AC Progress V2 high precision CNC WEDM" manufactured by "Agie-Charmilles Technologies Corporation" setup. "BroncoCut-X" wire (a new domain of zinc-coated copper wire) has been incorporated as an electrode on Cs, KW, and RA. The "BroncoCut-X" coated wire provides superior precision and cutting speed compared to the uncoated brass wire. Moreover, it requires less machine maintenance when compared to the gamma phase-coated wire, which has a tendency to produce "flaky and powdery" deposits on the WEDMed surfaces [24]. "Distilled water" has been used as dielectric media throughout the experiments. A resistivity meter continuously monitored the dielectric resistivity during the experiment. The straight polarity (i.e., workpart positive) has been selected during the investigation. The parameters for machining are chosen based on the available literature and the limitations of the WEDM machine. The performance of the "BroncoCut-X" wire has been evaluated in terms of Cs, KW, and RA.
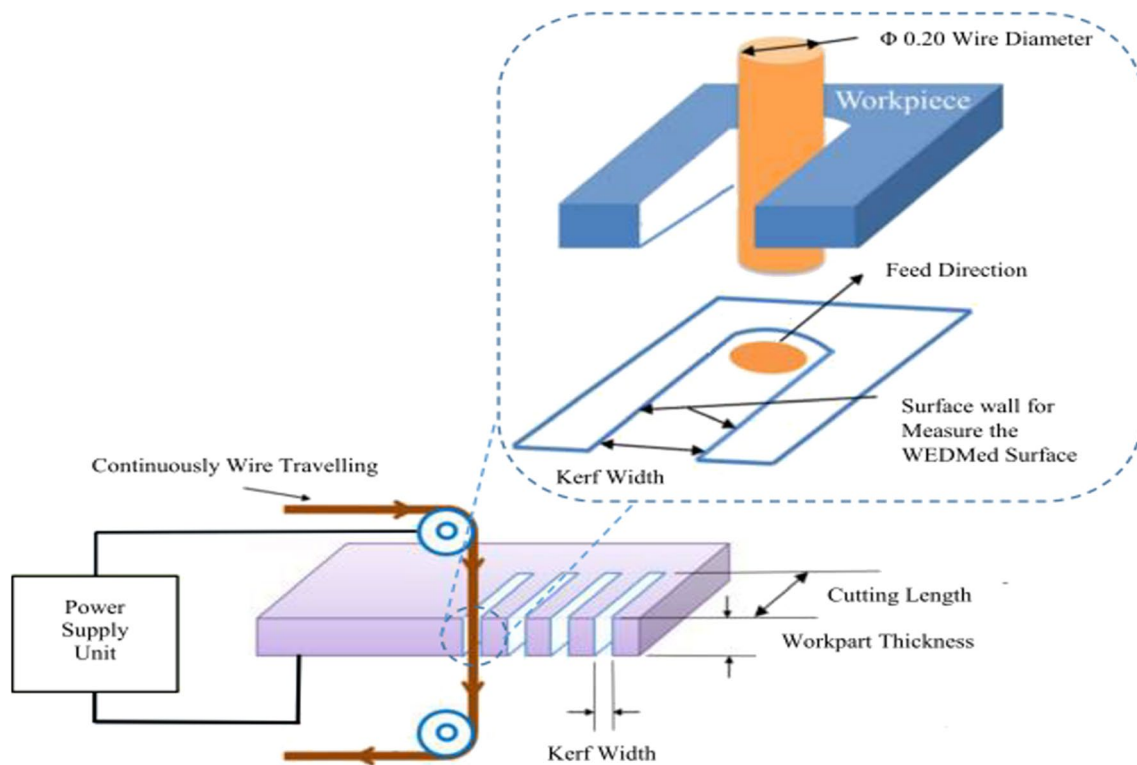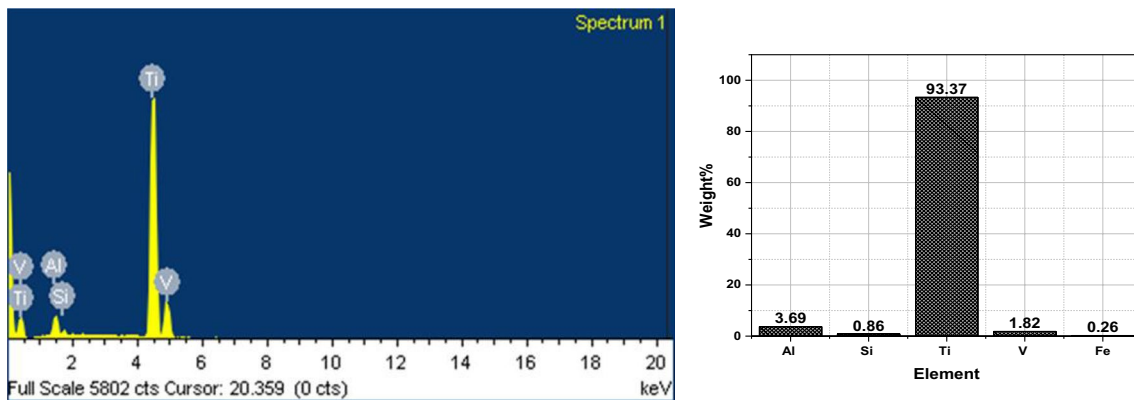
Fig. 1 schematic diagram of the Cutting process

Fig. 2 Elemental analysis of 'as received' workpiece

Table 1 Specifications of BroncoCut-X wire electrode

Specifications	Values
Core material	Copper
Coating material	CuZn50
Diameter (mm)	0.20
Tensile strength (MPa)	520
Elongation (%)	1

Source: https://www.bedra.com/en/products/bedraedm/broncocut-type-x/

Taguchi's L_{27} OA has been adopted for the experimental runs with five process parameters: T_w, S_w, P_f, I_d, and S_{on}. The details of the machining parameter and their levels are portrayed in Table 2. During the experimental run, a 10 mm cutting length is considered. The average of five observations from the various points of Cs is directly recorded from the inbuilt display monitor from the WEDM machine during the machining process. The snapshot of the KW was taken after the experimentation using a toolmaker microscope "(Carl Zeiss: JENA, Manufactured in GERMANY)". The

Table 2 Process factors and domain of variation

Notation	Parameters	Symbol	Level I	Level II	Level III	Unit
A	Wire Tension	T_w	10	13	16	N
B	Wire Speed	S_w	3	4	5	m/min
C	Flushing Pressure	P_f	8	12	16	[kg/mm^2]
D	Discharge Current	I_d	7	14	21	A
E	Spark-on Time	S_{on}	14	21	28	μs
Fixed-Parameter						
Spark-off Time		S_{off}	20			μs
Voltage		V	24			V
Polarity			Positive (+)			

measurement of KW is recorded from the installed microscope software. The undesired foreign material particles have been removed from the WEDMed surface before taking the reading from the surface texture meter ("Model: Talysurf 50, manufactured by Taylor Hobson Ltd., UK") for RA. On the WEDMed surface, the RA measurements have taken at four random locations. The averages of four location RA values have been used for analysis.

In addition, "Scanning Electron Microscopy (SEM)" ("Model: Nova Nano SEM 450") is employed for the morphology of the WEDMed surface. The surface was cleaned with the help of ultrasonic cleaning machining using acetone before being kept in the SEM machine.

Methodology Explore

In the manufacturing sectors, search for an optimum parameter to fulfil all types of conflict in nature criteria (means "Higher is the better" or "Lower is the better" criteria). It is challenging for industrial engineers to achieve the said condition characteristics simultaneously. It may be due to assumed mathematical complexity or computational time; even many metaphor-based algorithms have been used to solve such problems. Among that, many algorithms are not popular, or no one wants to use them due to the following reason; tuning parameter setting, complexity in mathematical equations, higher computational time, inefficiency, weight priority calculation etc. [25, 24]. This section explains the smart hybrid prediction tools called GRA-FIS coupled with Rao Algorithms (i.e., Rao1, Rao2, and Rao3) for WEDM responses. The framework of the experimental study and proposed optimization technique is shown in Fig. 3.

GRA- FIS Approach

This embedded approach transforms all experimental outcomes into scale-free responses and converts them to single-response data.

Grey relation analysis (GRA)

Grey relation grade was floated in 1985 by Wang Ting [26]. This technique aims to process the necessary data in such a way that makes possible decision-making. This technique has been explained briefly below.

This step converts all three conflicting machining responses value to a standard scale from 0 to 1. KW and RA are normalized using (equation (1)) as they are based on the "smaller the better" model, whereas Cs is normalized using (equation (2)) being based on the "larger the better" model.

$$Z_{pq} = \frac{Max(y_{pq}, p = 1, 2, ...n) - y_{pq}}{Max(y_{pq}, p = 1, 2, ...n) - min(y_{pq}, p = 1, 2, ...n)} \tag{1}$$

$$Z_{pq} = \frac{y_{pq} - min(y_{pq}, p = 1, 2, ...n)}{max(y_{pq}, p = 1, 2, ...n) - min(y_{pq}, p = 1, 2, ...n)} \tag{2}$$

Here $q = 1, 2, ...m$ and $P = 1, 2, ...n$, where m is the count of the responses studied, and the index n is the number of the experimental data parameter.

Fuzzy Interference System (FIS)

The FIS requires the present study to combine all outcome values from the GRA method. The FIS approach is very versatile to use in approximately every industrial problem. Lin et al. [27] used a fuzzy logic approach and reduced the machining error upto 50% more than the normal machining during the WEDM process. Shabgard et al. [28] determined that EDM and ultrasonic-assisted EDM processes used the fuzzy technique to predict tool wear rate, MRR and surface quality with a 90% and above prediction accuracy. This technique has shown its potential in a real-time application for fast processing time and is easy to adaptable [29]. This approach is considered to create a fuzzy model to remove the weight calculation by the decision-makers.
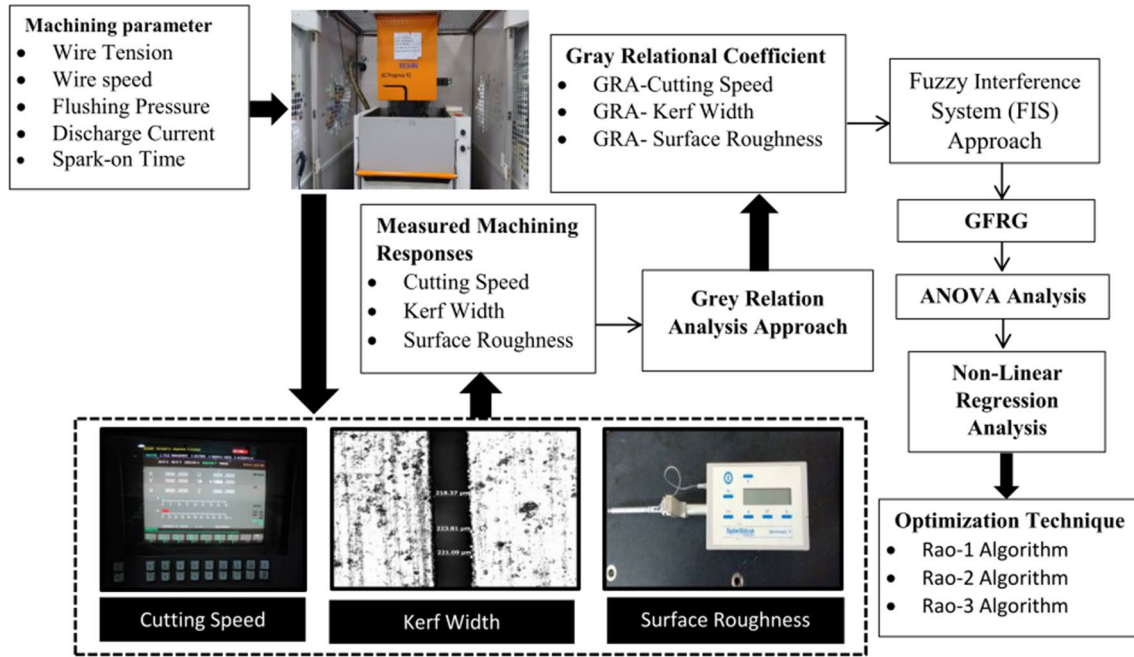
Fig. 3 The framework of experimental study and proposed optimisation route

Development of Mathematical Model

The non-linear regression model is a powerful static analysis tool for combining the mechanisms of variance analysis with regression analysis. This regression model is necessary and beneficial for the development of a mathematical model. The developed mathematical model is based on the correlation between the machining input and the machining responses. This mathematical model has been used to solve the multi-criteria decision problem in the present study. The mathematical models for the proposed process output characteristics that have been proposed are represented in (equation (3)).

$$Q_u = C \times Z_1^l \times Z_2^m \times Z_3^n \times Z_4^o \times Z_5^p \tag{3}$$

where, C = constant; $Z_1 = T_w$; $Z_2 = S_w$; $Z_3 = P_f$; $Z_4 = I_d$ and $Z_5 = S_{on}$; whereas $l, m, n, o,$ and p are estimated coefficients of the said regression model.

Rao Algorithms

Rao [30] developed three simple Rao Algorithms (i.e., Rao1, Rao2, and Rao3), which are more advanced new metaphor-less and algorithm-specific parameter-less algorithms to fix the said issue in Sect. "Methodology Explore". The Rao algorithm works on two identification of solutions. The first is the BEST solution, and the second is the WORST solution in the entire population via random interactions (during

$'g'$ iterations of optimal search corresponding to decision variables. In this study, the fitness function (q) needs to be maximized to proceed with the optimization problem. The identification of fitness function from n population of best and worst solution can be represented as q_{best} and q_{worst} respectively. The value of $M_{e,f,g}$(where the value of eth variable corresponds to f^{th} the candidate during g^{th} iteration) is modified according to the following (equation. (4)).

$$M_{e,f,g}^* = M_{e,f,g} + rand_{1,e,f,g}\left(M_{best,f,g} - M_{worst,f,g}\right) \tag{4}$$

$$M_{e,f,g}^* = M_{e,f,g} + rand_{1,e,f,g}\left(M_{best,f,g} - M_{worst,f,g}\right) \\ + rand_{2,e,f,g}\left(|M_{e,f,g} \text{ or } M_{E,f,g}| - |M_{E,f,g} \text{ or } M_{e,f,g}|\right) \tag{5}$$

$$M_{e,f,g}^* = M_{e,f,g} + rand_{1,e,f,g}\left(M_{best,f,g} - M_{worst,f,g}\right) \\ + rand_{2,e,f,g}\left(|M_{e,f,g} \text{ or } M_{E,f,g}| - (M_{E,f,g} \text{ or } M_{e,f,g})\right) \tag{6}$$

Terms $rand_1$ and $rand_2$ are made up of random numbers between 0 and 1. $M_{e,f,g}$ and $M_{E,f,g}$ represent the eth candidate solution in comparison to the random E^{th} candidate solution and exchange fitness value information with the help of (equations (5) and (6)). If the fitness function value of eth the candidate solution shows a superior function value than E^{th}, then $M_{e,f,g} \text{ or } M_{E,f,g}$ change to $M_{e,f,g}$ and $M_{E,f,g} \text{ or } M_{e,f,g}$ convert to $M_{E,f,g}$. On the other hand, if the fitness function value q_K produced a satisfactory solution than q_k the candidate solution value, then the $M_{e,f,g} \text{ or } M_{E,f,g}$ converts to be $M_{E,f,g}$ and

$M_{E,f,g}$ or $M_{e,f,g}$ turns to $M_{e,f,g}$. Equation (4) is utilized for the Rao1 method, (equation (5)) is used for the Rao2 algorithm, and (equation (6)) is used for the Rao3 algorithm in order to achieve optimal global solutions. The obtained global optimal solution from the Rao algorithm, JAYA and I-GWO are compared to fitness value and time for algorithm performance. Figure 4 shows the overview of the Rao-1 algorithm.

Results and Discussions

This section explores the experiment data to identify the effects of wire electrodes using machining parameters on the machining outputs characteristics. The measurement of KW is depicted in Fig. 5. The experiment results are depicted in Table 3.

SEM Analysis of WEDM

Figure 6 shows the details of the surface characteristics analysis of WEDMed Ti-3Al-2.5 V with mentioned process parameter conditions (See Table 3). The texture of the WEDMed surface showed unfair observation due to the appearance of the deposition of melted material, spherical droplets, microcracks, craters, unevenly deposited debris, and pockmarks. The melted materials are clustered in large sizes on the WEDMed surface, which gives an uneven surface. It may have happened due to the high value of S_{on} generated maximum spark time for discharge energy which is responsible for the melting and evaporating process during the machining [31]. The spherical droplets may have been made because the dielectric fluid rapidly cooled down the vaporized material and then solidified
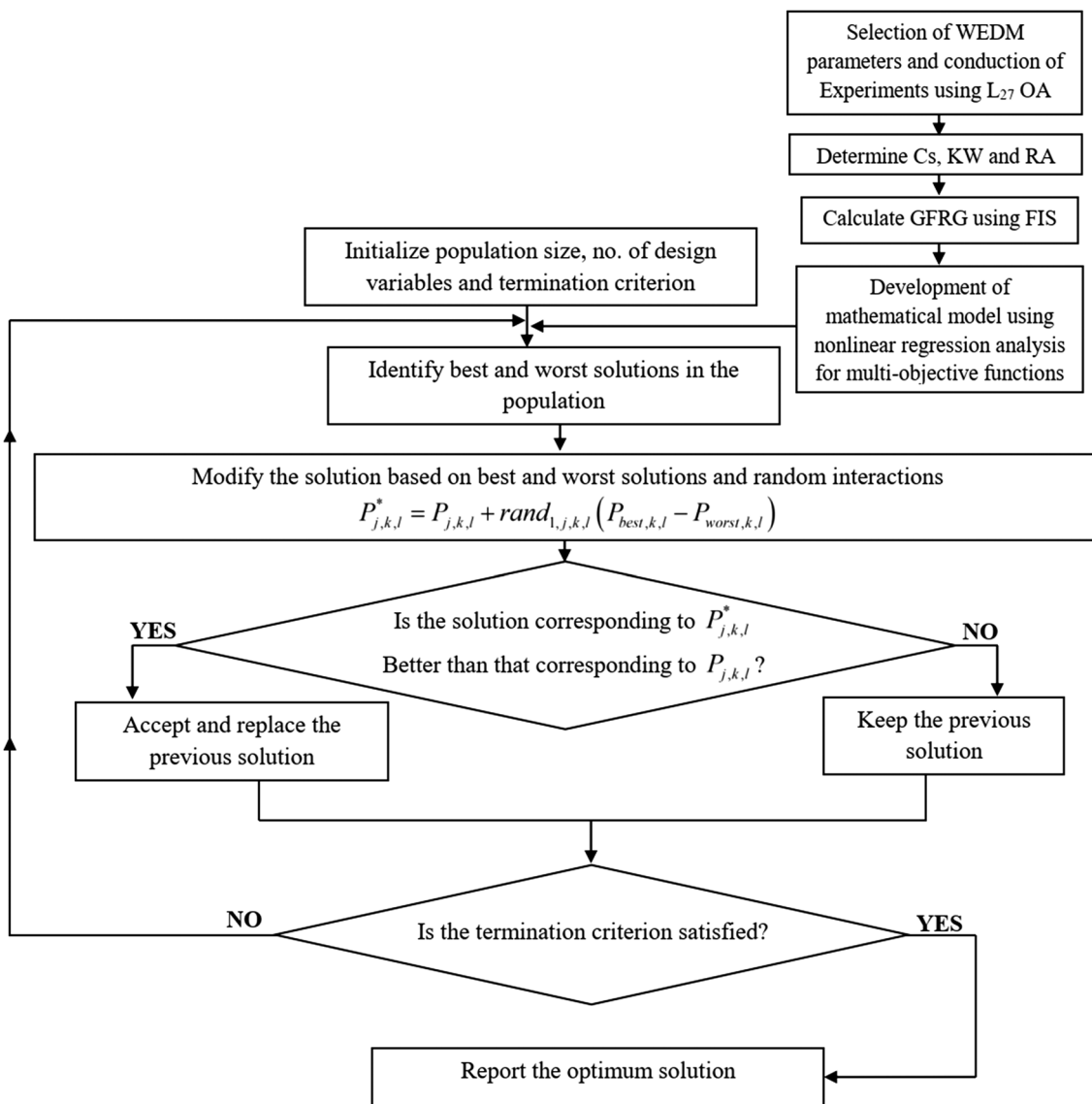

Fig. 4 Flowchart of the proposed optimisation route for Rao-1

Fig. 5 KW measurement (See Table 3)

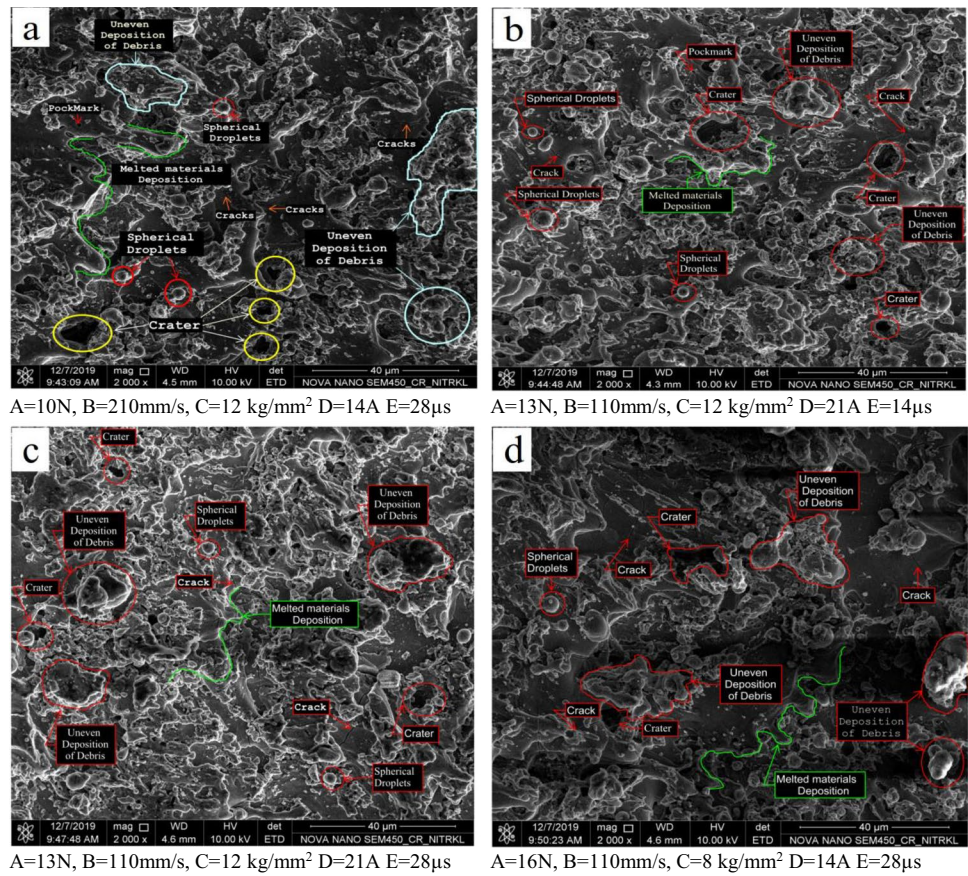**Run no. 3**　　　　　**Run no. 23**

Table 3 Experimental data

Sl. No	A	B	C	D	E	Cs (mm/min)	KW (mm)	RA (µm)
1	1	1	1	1	1	4.15	0.2265	4.04
2	1	1	1	1	2	3.95	0.2249	4.22
3	1	1	1	1	3	4.73	0.2218	4.75
4	1	2	2	2	1	5.20	0.2317	4.36
5	1	2	2	2	2	5.78	0.2398	4.52
6	1	2	2	2	3	7.62	0.2392	5.41
7	1	3	3	3	1	4.02	0.2226	3.94
8	1	3	3	3	2	3.80	0.2277	4.41
9	1	3	3	3	3	4.30	0.2282	4.71
10	2	1	2	3	1	6.80	0.2330	4.13
11	2	1	2	3	2	6.70	0.2663	4.47
12	2	1	2	3	3	8.90	0.2601	4.92
13	2	2	3	1	1	3.85	0.2271	3.94
14	2	2	3	1	2	3.74	0.2327	3.99
15	2	2	3	1	3	4.46	0.2287	4.62
16	2	3	1	2	1	4.63	0.2376	3.94
17	2	3	1	2	2	4.58	0.2381	3.81
18	2	3	1	2	3	5.46	0.2312	4.63
19	3	1	3	2	1	7.50	0.2242	5.67
20	3	1	3	2	2	7.36	0.2255	5.94
21	3	1	3	2	3	8.58	0.2248	6.62
22	3	2	1	3	1	7.04	0.2595	4.66
23	3	2	1	3	2	6.90	0.2284	4.06
24	3	2	1	3	3	7.90	0.2242	4.52
25	3	3	2	1	1	4.30	0.2291	3.34
26	3	3	2	1	2	4.49	0.2351	3.36
27	3	3	2	1	3	5.37	0.2274	4.03

again [32]. The creation of pockmarks may because by the solidification of gas bubbles ejected from molten material. The dielectric water offers rapid quenching of molten material, resulting in the present gas bubbles solidifying before it grows up to maximum. Therefore, the size of pores is observed very little. Above all, such micro-voids may hinder the effective tensile strength of the WEDMed surface, resulting in surface cracks appearing on the machined surface [33].

The importance of "BroncoCut-X" validates inference through the zinc-coated wire electrode. The zinc layered wire provide the higher Cs. This is due to the capability of the zinc layer to sustain high discharge energy and improved flushability. Due to the low melting and evaporation temperature of the zinc layer, the conductivity in the machining zone increases and improves flushability [24]. To accurately identify the recast layer thickness under different no-load rates, the WEDMed samples have been ultrasonically cleaned, polished, and treated with reagent corrosion prior to capturing SEM snapshots. Figure 7(a–b) depicted the SEM images of the cross-sectional area of the WEDMed

Fig. 6 Morphology of the machined surface

A=10N, B=210mm/s, C=12 kg/mm² D=14A E=28μs

A=13N, B=110mm/s, C=12 kg/mm² D=21A E=14μs

A=13N, B=110mm/s, C=12 kg/mm² D=21A E=28μs

A=16N, B=110mm/s, C=8 kg/mm² D=14A E=28μs

sample. The recast layer is obtained under various cutting settings. During the spark, some parts of the workpart get melted. The bombardment of high-velocity electrons at the workpart causes the erosion process. The dielectric fluid is used for flushing eroded debris. Inadequate flushing may result in the re-solidification of debris over the machined surface, resulting in the formation of a recast layer. Here, recast layer thickness has been observed to vary in the range from 4.89 μm to 8.36 μm at 14 μs (S_{on}) and 2.02 μm to 8.84 μm at 21 μs (S_{on}). Similar findings were observed by Zahoor et. al. [24] regarding the improvement of recast layer thickness using BroncoCut-X wire.

Parametric Significance Analysis

In this section, the parametric significance of analysis has been done using "Analysis of variance" (ANOVA). The ANOVA has been determined using MINITAB® 19. The Percentage Contribution Ratio (PCR) is calculated for each process parameter. The analysis of variance (ANOVA) is a statistical approach that can be used to determine the adequacy and significance of a parametric effect and estimate the probability of accuracy given the results of the tests [16, 34]. A confidence interval of 95% is used to determine the parametric significance of this study. The results are reported

for each machining outcome in Table 4. The PCR is a tool for determining the influence of machining parameters on responses. In this case, PCR is used to evaluate and prioritize the significance of machining parameters in relation to machining outcomes. The percentage of contribution (PCR) has been reported in Fig. 8.

The effect of T_w, S_w, P_f, I_d, and S_{on} on Cs is rated as significant. Among the mentioned significant machining variables I_d shows a prominent PCR value of 34.91%. The PCR value of T_w, S_w, P_f, and S_{on} on Cs is observed as 23.48%, 3.77%, 6.64%, and 8.52%, respectively are considered as less significant parameters. The leading PCR value for KW is observed as P_f with 41.36%. The PCR value of T_w, S_w, I_d, and S_{on} is reported on KW as 35.85%, 3.77%, 12.47%, and 3.97%, respectively are considered as less significant parameter. S_w is the most contributing parameter for RA, with a PCR value of 34.15%. It is noticed that I_d is the second most contributing control parameter for the mentioned response attribute with a PCR of 29%.

The coefficient of determination (R^2) symbolizes how closely the data fit with the model. The highest R^2 value indicates that it is acceptable and suitable for estimating the aforementioned machining results. The R^2 value for Cs has been observed as 99.07%, followed by KW and RA as 97.42% and 97.18%, respectively.
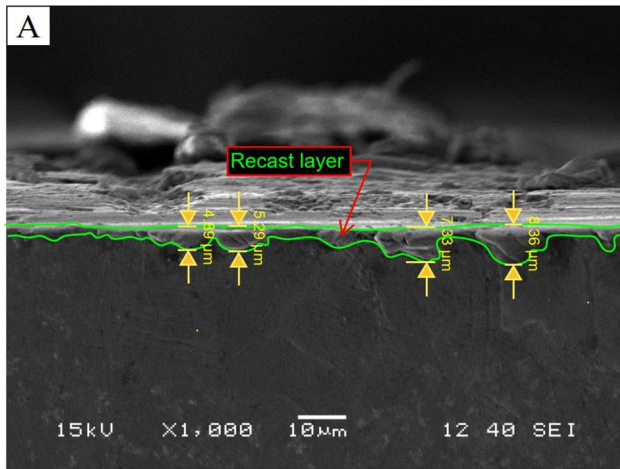
A=16N, B=110mm/s, C=16 kg/mm² D=14A E=14μs
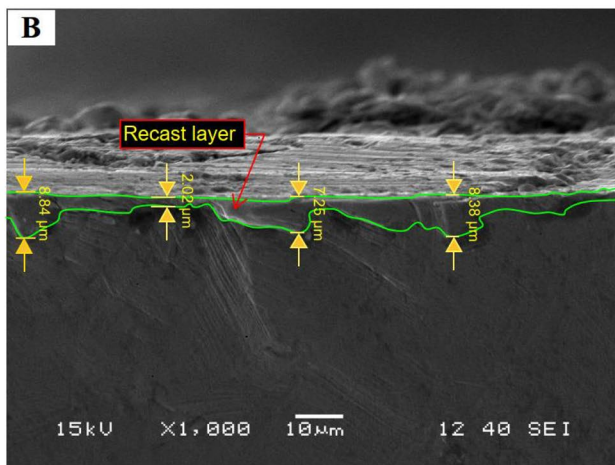
A=16 N, B=110 mm/s, C=16 kg/mm² D=14A E=21μs

Fig. 7 Recast layer as observed in cross-section of WEDMed sample

Process Parametric Effects Analysis

In this section, parametric process analysis has been done from mean effect plot to identify the behaviour of process parameters using a graphical representation of machining responses. The behaviour analysis results are based on statistical analysis.

Cutting speed

The maximum value of Cs is observed at 8.90 mm/min for straight cut by "BroncoCut-X" wire. A similar type of literature reported, where highest Cs is observed as 3.998 mm/min using BroncoCut-X wire electrode [24]. The vaporization of zinc coating in BroncoCut-X helps to maintain lower temperature of wire core, which permits use of more intensive pulse power and results in increased cutting speed. It is a predictable behaviour consistent with the literature [17, 24, 35].

The parametric influences on Cs are graphically depicted using the main effect plot in Fig. 9. Figure 9(a) shows a prominent rise in Cs (from 4.75 mm/min to 6.578 mm/min) reported at high level of T_w. This is due to the increased value of T_w gives a strong force on the wire electrode, which provides wire stability during the machining. The stability of the wire provides better sparking phenomena in the working gap [36]. Moreover, it has been noticed that a higher level of S_w shows an inverse trend in the Cs (from 6.55 mm/min to 4.55 mm/min), which is demonstrated in Fig. 9(b). The incremental value of S_w is responsible for the shorter spark cycle in the small machining zone hence, lower Cs. Additionally, lower S_w is always preferred because it favours economical machining [37]. Figure 9(c) shows that Cs increase from 5.46 mm/min to 6.07 mm/min with an increase in the P_f from level 1 to level 2. The low P_f promotes the transmission of thermal energy of spark from the wire electrode to the workpart due to increased ionization of the dielectric medium with fixed spark-off time., hence increase Cs.On the contrary, when the variable increases from level 2 to level 3, Cs decreases from 6.07 mm/min to 5.29 mm/min. This may be validates that the increasing P_f increase the volum of the dielectric fluid in the machining zone, which increase the wire deflections causing a reduction

Table 4 ANOVA Table for Cs, KW and RA

| Source	Sum of Squares (SS)			Degrees of Freedom (DF)			Mean Square (MS)			F-Ratio			PCR (%)		
	Cs	KW	RA	Cs	KW	RA	Cs	KW	RA	Cs	KW	RA	Cs	KW	RA
A	34.694	1.8025	0.7300	2	2	2	17.35	0.90125	0.3650	200.96	111.11	4.320	23.48	35.85	1.52
B	37.708	0.1895	16.371	2	2	2	18.85	0.09474	8.1856	218.42	11.680	96.85	25.52	3.77	34.15
C	09.813	2.0798	6.3422	2	2	2	4.910	1.03990	3.1710	56.840	128.20	37.52	06.64	41.36	13.23
D	51.594	0.6268	13.900	2	2	2	25.80	0.31341	6.9501	298.85	38.640	82.23	34.91	12.47	29.00
E	12.589	0.1998	9.2401	2	2	2	6.290	0.09990	4.6200	72.920	12.320	54.66	08.52	3.97	19.28
Residual	01.381	0.1298	1.3523	16	16	16	0.086	0.00811	0.0845				0.93	2.58	2.82
Total	147.779	5.0282	47.936	26	26	26							100	100	100
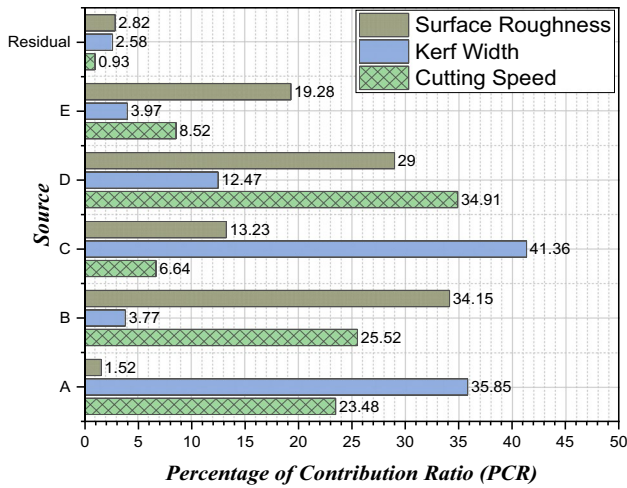
Fig. 8 Percentage Contribution Ratio for Cs, KW, and RA

in the striking spark intensity and hence lower Cs. As noticed in Fig. 9(d) and (e) that both I_d (i.e., from 5.256 mm/min to 6.258 mm/min) and S_{on} (i.e., from 4.34 mm/min to 6.262 mm/min) are significantly influencing the Cs during WEDM of Ti-3Al-2.5 V. A prominent rise in Cs has been reported at a high level of the two control parameters. However, the I_d holds a more influential role in governing the magnitude of Cs as compared with S_{on}. Basically, increasing the action of I_d and S_{on} of boosted discharge energy facilitates the action of material evaporation rate, which improves the impulsive force in the cutting zone. Therefore Cs upsurges noticeably [32].

Kerf width

KW is an important attribute in WEDMed process. It directly affects the precision and material utilization of the workpart and the inside corner radius of the product. The analysis

Fig. 9 Main effect plot on Cs
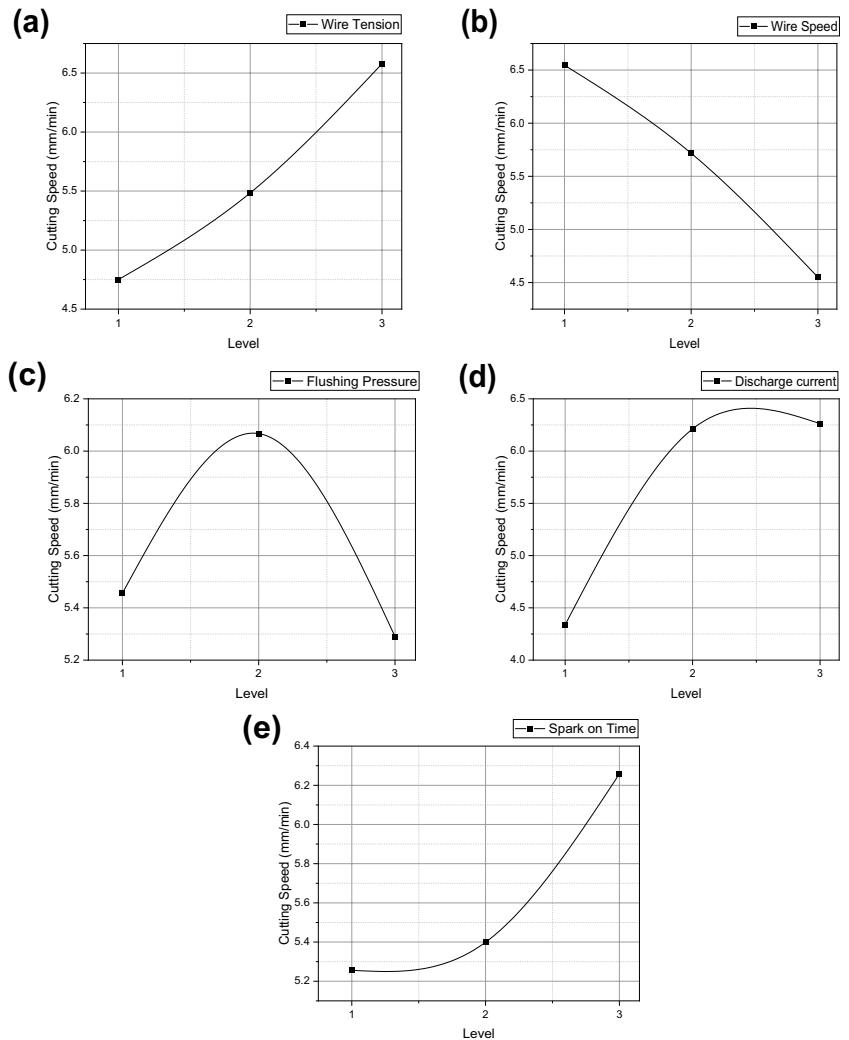
of the parametric effects on the KW is stated in Fig. 10. Figure 10 (a) shows that when the value of T_w increases from level 1 to level 2, the KW increases upto its maximum value (i.e., 0.2424 mm). This enhancement is attributed to the lower value of T_w is responsible for higher wire amplitude which generates uneven arcing in the machining zone, resulting in higher KW. On the other hand, when the value of T_w reaches level 3, the amplitude of the wire is controlled by the applied stretches subjected to two forces. This causes the wire diameter to decrease, which affect decreases in the spark gap between the wire and workpart. Therefore, more debris accumulates in the spark gap. This results in melting lower amounts of target material which results in narrow KW (i.e., 0.2266 mm) [38]. However, Fig. 10(b) presented that increasing the S_w from level 1 to level 3 decreased the KW from 0.2359 mm to 0.2308 mm. This may occur due to the small amount of flushing process that occured in the working gap. Thus, the flushing of byproducts of the workpart also goes down. This may cause more contamination in the working gap with sub-microparticls of zinc, making the ionization channel faster and consequently more regular

sparks that increase the kerf width. Reolon et al. [19] also observed this type of behavior. Figure 10(c) shows that when the P_f increases from level 1 to level 2, then KW increases from 0.2270 mm to 0.2431 mm. It is also observed that KW decrease to its minimum at level 3 (i.e., 0.2268 mm). The rising trend could be due to the fact that when P_f reaches level 2, then the proper flushing of the dielectric ensures the removal of a considerable quantity of debris, thus, in turn, enlarging KW. On the other hand, when the P_f reaches level 3, the amplitude of the wire may increase due to dielectric pressure, which decreases the spark gap. Therefore, it is difficult for the deionized water to get into the narrow working gap. Residues of debris adhered at the WEDMed surface resulted in minimum KW. Figure 10(d) observed that when the I_d increases from level 1 to level 3, then the KW also increases from 0.2270 mm to 0.2375 mm. The observed phenomenon can be attributed to an increase in the level of I_d, which increases the spark energy in the spark gap. A larger heat flux to be introduced into the work surface, which removes high material from the working zone and produces wider KW. Figure 10(e) shows that when S_{on} increases

Fig. 10 Main effect plot on KW
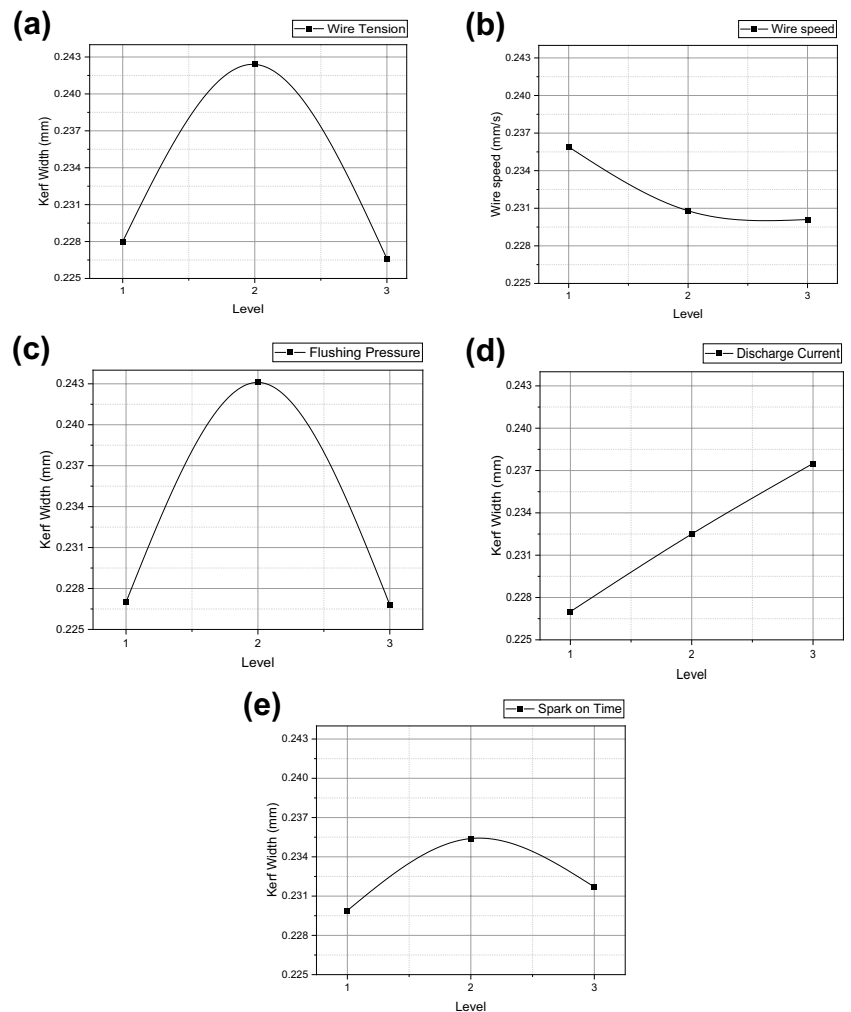
from level 1 to level 2, the KW increases from 0.2299 mm to 0.2354 mm, and afterwards, the KW decreases upto 0.2317 mm at level 3. Increasing S_{on} (from level 1 to level 2) amplifies the discharge energy to the working gap, which in turn removes more material in the target material, resulting in a widening of the WEDMed KW [34]. Furthermore, when S_{on} gradually increases to level 3, then KW decreases. This behaviour is because the discharge energy increases with increasing the S_{on}, resulting in a more uniform distribution of sparks during the process. As a result, the magnitude of the KW is reduced [39].

Surface roughness

RA represents the quality of WEDMed end product and varies significantly over the range of machining parameters. Figure 11 describes the main effects plots for RA obtained during WEDM. Figure 11(a) reveals that with an increase in T_w from level 1 to level 2, the value of RA decreases from 4.484 μm to 4.331 μm. But when T_w increases further, the value of RA increases upto 6.632 μm. The increase of T_w decreases the average wire amplitude. However, it increases the circulation of dielectric fluid along the wire circumference to better flushing, resulting in a decrease in RA. Furthermore, RA is amplifying at level 3 of T_w with other parameters that have been kept constant. With a higher value of T_w, the wire tends to be more rigid, and the length of active cutting is shorter. This may interrupt the ionization of the dielectric medium, which causes the spark intensity striking the surface to increase. This leads to the re-deposition of the debris [40]. However, in Fig. 11(b) observed that increasing S_w produces less surface irregularities on the WEDMed surface. It may be because the wire electrode has a shorter contact time with the workpart. As a result, the dielectric flushes more debris/melted material and

Fig. 11 Main effect plot on RA
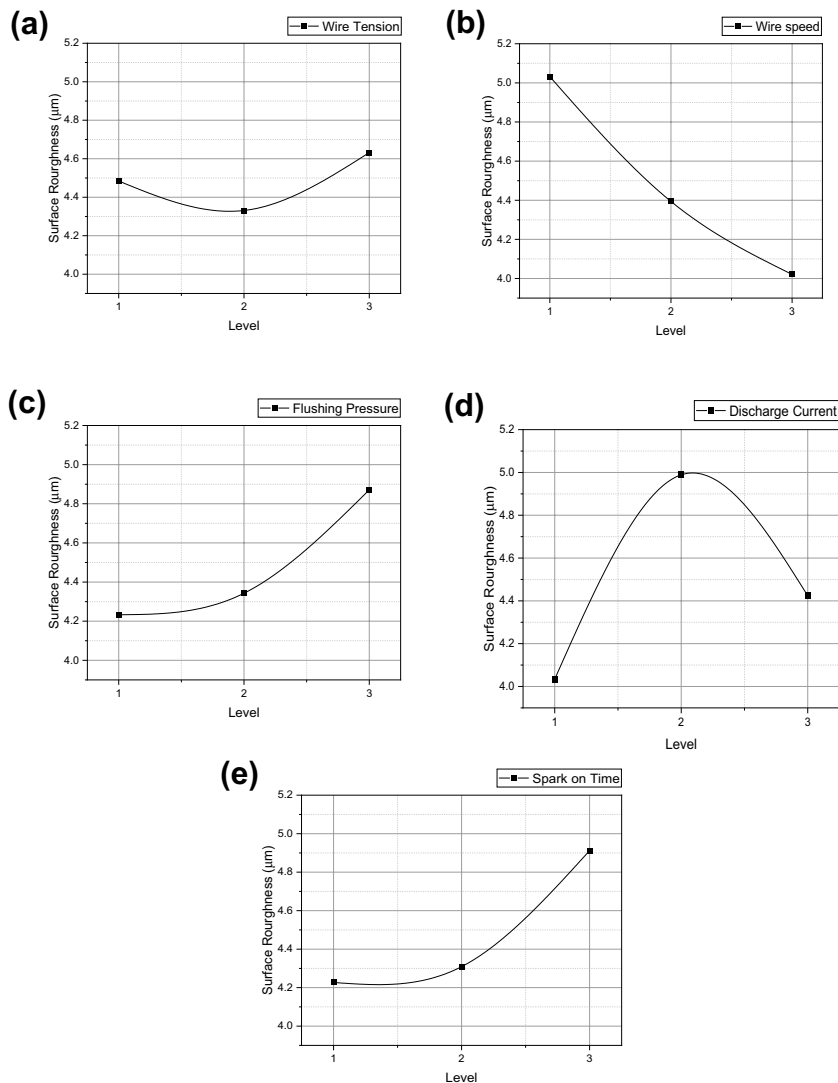
produces less irregularities on WEDMed surface, which gives a minimum RA. Furthermore, it can be determined that the incoming wire contributed to the reduction of thermal energy within the machining zone (in terms of heat transfer and plasma generation). This low discharge energy caused less deterioration of WEDMed surface. As previously observed by Zahoor et al. [24] and Somashekhar et al. [41]. Figure 11(c) shows that when the P_f increases from level 1 to level 3, the RA increases from 4.233 μm to 4.871 μm. The higher level of P_f increases the kinetic energy of the injected dielectric fluid, which cause a strong deflection force on the moving wire electrode. This may hinder the uniform electro-erosive erosion of the workpart, which led to a rapid re-deposition of the debris on the WEDMed surface. This inferior surface profile is also verified from Fig. 6. Figure 11(d) shows the parametric influences of I_d on RA. The RA increases (i.e., from 4.034 μm to 4.424 μm) with an upsurging of the variable from level 1 to level 2. Such behaviour might

be attributed to I_d with all other parameters kept constant, generating high pulse energy and impinges on the workpart. This high energy is responsible for the evaporation and melting process during machining, which forms a deeper crater on the WEDMed surface and leading to a coarser surface. On the other hand, RA decrease when the I_d goes to level 3. It may be justified that, at level 3, the molten material achieves sufficient temperature to evacuate from the machined surface, resulting in a decrease in RA. Additionally, "BroncoCut-X" wire has excellent flushabilty phenomena effects during machining. Figure 11(e) shows that high values of S_{on} are associated with an increased RA from 4.227 μm to 4.912 μm. It is a reasonable fact that the gradual increase of S_{on} gives a longer interaction time of spark between the wire electrode and workpart during machining. Consequently, considerable heat is accelerated in the machining zone, leading to a rapid rate of material evaporation from the WEDMed surfaces and the formation of deeper craters. Conversely, the

Table 5 Normalized value of experimental results using GRA and GFRG value

Sl No.	Normalized Values			Grey Relational Coefficient			GRG	GFRG
	N-CS	N-KW	N-RA	G-CS	G-KW	G-RA		
1	0.079	1.000	0.786	0.352	1.000	0.700	0.684	0.747
2	0.041	0.831	0.731	0.343	0.748	0.651	0.580	0.659
3	0.192	0.904	0.571	0.382	0.838	0.538	0.586	0.701
4	0.283	0.695	0.689	0.411	0.621	0.617	0.549	0.649
5	0.395	0.532	0.640	0.453	0.517	0.582	0.517	0.694
6	0.752	0.544	0.370	0.668	0.523	0.442	0.545	0.682
7	0.054	0.878	0.817	0.346	0.803	0.732	0.627	0.694
8	0.012	0.775	0.674	0.336	0.690	0.605	0.544	0.644
9	0.109	0.765	0.581	0.359	0.680	0.544	0.528	0.649
10	0.640	0.137	0.597	0.581	0.367	0.554	0.500	0.778
11	0.574	0.000	0.655	0.540	0.333	0.591	0.488	0.763
12	1.000	0.124	0.519	1.000	0.364	0.510	0.624	0.742
13	0.021	0.787	0.817	0.338	0.701	0.732	0.590	0.662
14	0.000	0.675	0.802	0.333	0.606	0.716	0.552	0.649
15	0.140	0.755	0.610	0.368	0.671	0.562	0.533	0.643
16	0.172	0.576	0.819	0.377	0.541	0.734	0.551	0.674
17	0.163	0.566	0.856	0.374	0.535	0.777	0.562	0.682
18	0.333	0.705	0.608	0.429	0.629	0.561	0.539	0.644
19	0.729	0.845	0.290	0.648	0.764	0.413	0.608	0.675
20	0.702	0.819	0.206	0.626	0.735	0.387	0.582	0.651
21	0.938	0.833	0.000	0.890	0.750	0.333	0.658	0.731
22	0.593	0.922	0.760	0.551	0.865	0.676	0.697	0.761
23	0.612	0.761	0.779	0.563	0.677	0.694	0.645	0.649
24	0.806	0.845	0.642	0.721	0.764	0.583	0.689	0.689
25	0.109	0.747	1.000	0.359	0.664	1.000	0.674	0.740
26	0.145	0.627	0.994	0.369	0.572	0.988	0.643	0.746
27	0.316	0.781	0.789	0.422	0.696	0.703	0.607	0.657

GRG Gray Relation Grade; *GFRG* Grey Fuzzy Reasoning Grade

Table 6 Fuzzy rule matrix

Rule No.	Cs (IF)	KW (IF)	RA (IF)	THEN (GFRG)
1	Low	Low	Low	Very Low
2	Low	Low	Medium	Low
3	Low	Low	High	Medium
4	Low	Medium	Low	Very Low
5	Low	Medium	Medium	Low
6	Low	Medium	High	Medium
7	Low	High	Low	Low
8	Low	High	Medium	Low
9	Low	High	High	Medium
10	Medium	Low	Low	Low
11	Medium	Low	Medium	Medium
12	Medium	Low	High	High
13	Medium	Medium	Low	Low
14	Medium	Medium	Medium	Medium
15	Medium	Medium	High	High
16	Medium	High	Low	Medium
17	Medium	High	Medium	Medium
18	Medium	High	High	High
19	High	Low	Low	Medium
20	High	Low	Medium	High
21	High	Low	High	Very High
22	High	Medium	Low	Medium
23	High	Medium	Medium	High
24	High	Medium	High	Very High
25	High	High	Low	High
26	High	High	Medium	High
27	High	High	High	Very High

faster evaporation process adversely affects the flushing process, resulting in the re-deposition of melted material on the WEDMed surface [24]. This argument has also been validated by SEM micrographs shown in Fig. 6. Furthermore, the smaller value of RA is achieved at 3.34 μm. Zahoor et al. [24] revealed approximately the same result in terms of RA.

Careful examination of Figs. 9, 10 and 11 appears that the best level of the significant factor for Cs, KW, and RA are $A_3B_1C_2D_3E_3$, $A_3B_3C_3D_1E_1$, and $A_2B_3C_1D_1E_1$, respectively. The results confirm that the machining outcomes (i.e., Cs, KW, and RA) are completely contradictory. Therefore, a suitable strategy has to develop to identify the globally optimal solution for this study.

Mathematical Modelling and Proposed Optimisation Technique

In this section, strategy has been taken for the machining parameter optimal global solution using Grey-Fuzzy based metaphor-less algorithms (i.e., Rao algorithms) using PYTHON Version 3.10.2 and executed on a computer (HP Intel (R) Core (TM) i3-7100U processor CPU at 2.40 GHz and RAM: 4 GB).

In this hybrid approach, the first to convert experimental responses (i.e., Cs, KW, and RA) into the normalized individual value using the GRA technique (using Eqs. (i)-(iv)) (see Table 5). The second step is to convert the normalized value into fuzzy crisp output (i.e., GFRG) using FIS and consider it as an output response. In the FIS "Mamdani" type is used to

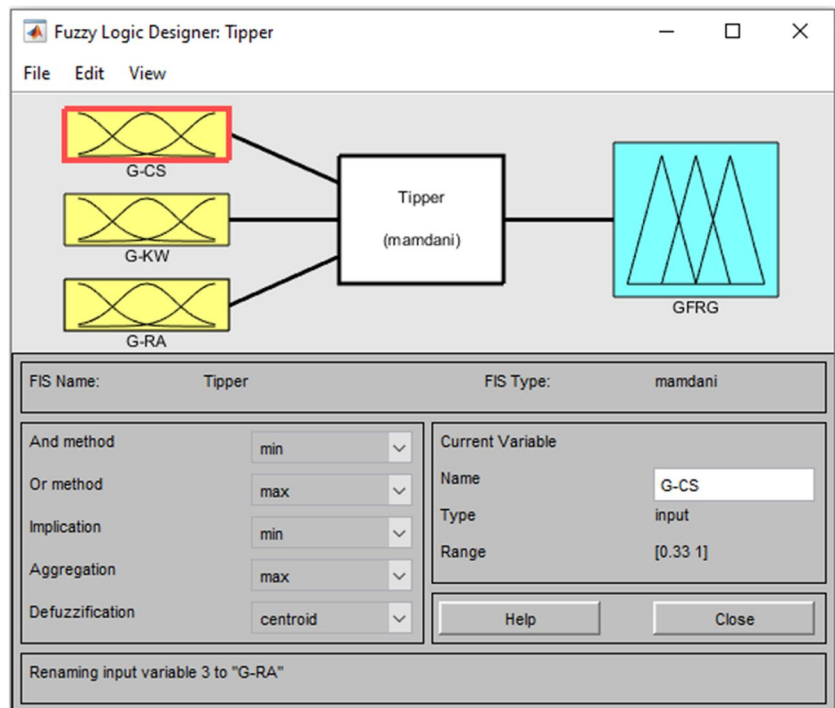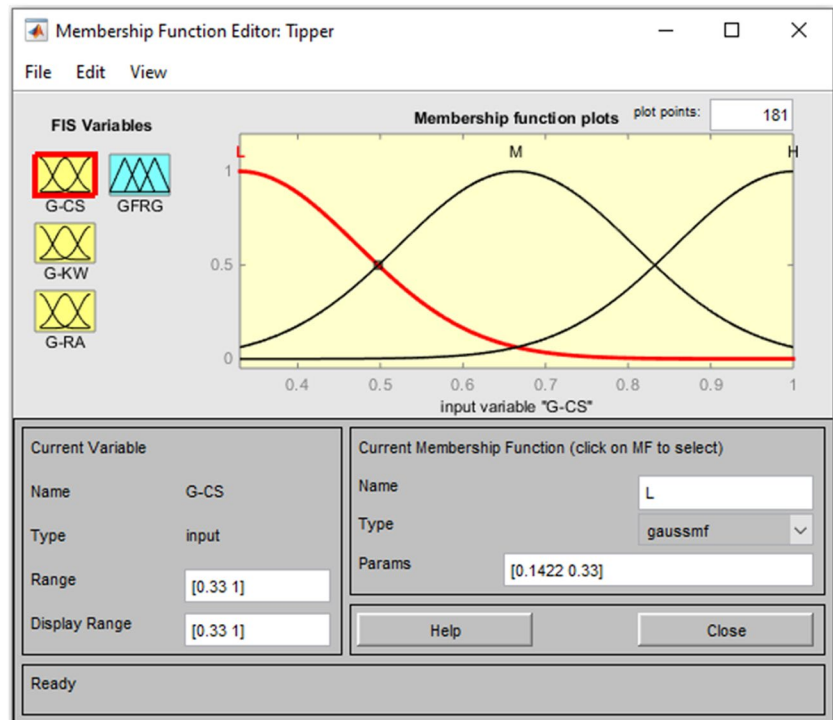**Fig.12** fuzzy inference system (FIS) architecture

Fig. 13 Membership function for G-KW

develop the membership function (MF) considered for each input and output variable of the fuzzy set. Fuzzy subsets have been expressed into "Low", "Medium," and "High" sections, whereas outcome (GFRG) has been shown as five MF viz. "Very Low (VL)", "Low (L)", "Medium (M)", "High (H)" and "Very High (VH)" (see Table 6) (Figs. 12, 13 and 14).

The ANOVA is carried out so that the significance and suitability of the mathematical model for GFRG can be reaffirmed. Here, the insight of the ANOVA test of GFRG is

Fig. 14 Fuzzy rule editor

in Table 7. The trend of the R^2 value for GFRG displayed as 94.63% and is found adequate. The highest value of R^2 (i.e., GFRG) indicates that the model has better goodness of fit, and it can be used to identify the fitness function for Rao algorithms. The percentage contribution of individual machining parameters for GFRG has been portrayed in Fig. 15. It has been observed that S_w has more contribution (i.e., 46.86%) than the rest of the machining parameters. The second most important parameter is considered to be S_{on} (14.87%). The P_f is found to be the least important parameter, with a PCR value of 8.64% among the selected parameters. Non-linear regression analysis is utilized to establish the mathematical model for single machining outputs (i.e., Cs, KW, and RA) and multi-responses (i.e., GFRG) to identify the fitness functions depicted in equations (7-10). The comparison plot (see Fig. 16) between GFRG and GRG for all the experimental runs. Fig. 16 observed the improvement in the value of GFRG compared with GRG for all the experiment runs. This reduces the uncertainty of the data, and the grade value is closer to the reference value of 1. Thus, it validated the robustness of empirical models.

However, the JAYA algorithm has also been applied for obtaining the optimum solution and found the same parametric setting with the same fitness function value. The convergence plots for Rao-1, Rao-2, Rao-3, JAYA, and Improved-Grey wolf optimizer (I-GWO) (invented by Mirjalili et. al. [42]) have been portrayed in Figs. 17, 18, 19, 20 and 21 correspondingly.
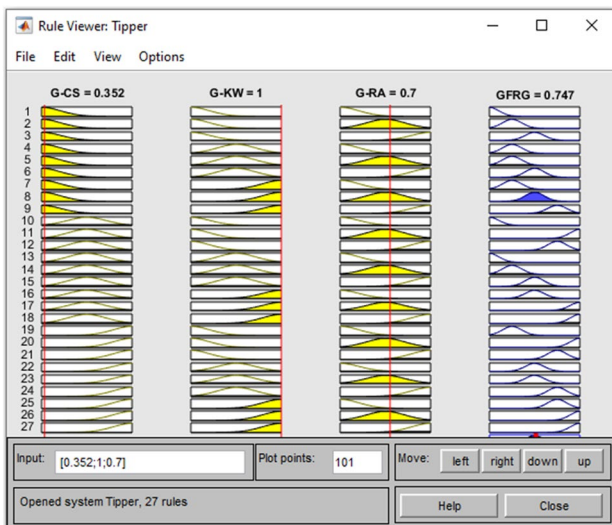
Table 7 ANOVA and PCR analysis for GFRG

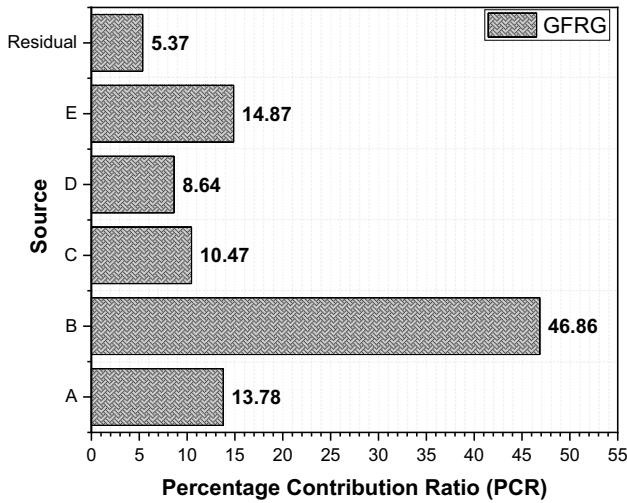| Source	Sum of Squares (SS)	Degrees of freedom (DF)	Mean Square (MS)	F-Ratio	PCR (%)
A	10.031	2	5.0157	20.52	13.78
B	34.099	2	17.0495	69.77	46.86
C	7.623	2	3.8113	15.60	10.47
D	6.286	2	3.1432	12.86	08.64
E	10.821	2	5.4106	22.14	14.87
Residual	3.910	16			05.37
Total	72.771	26			100

Fig. 15 Percentage Contribution Ratio for GFRG
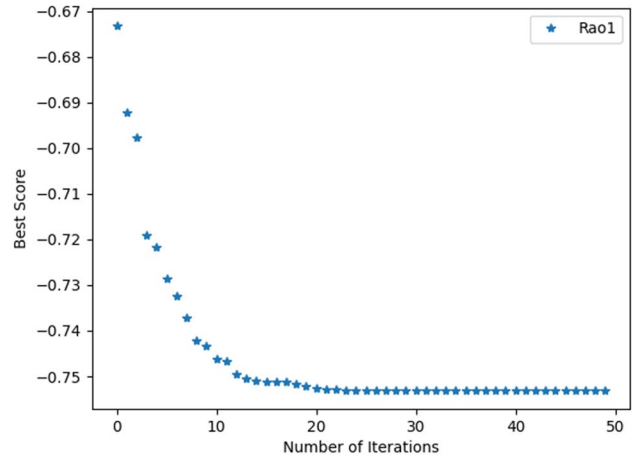
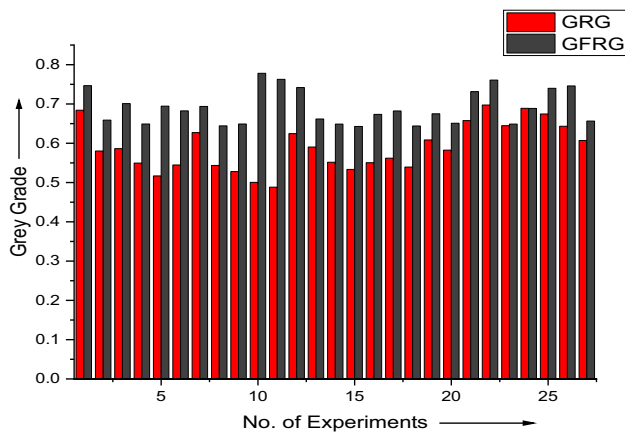**Fig. 17** Convergence curve for GFRG based Rao-1

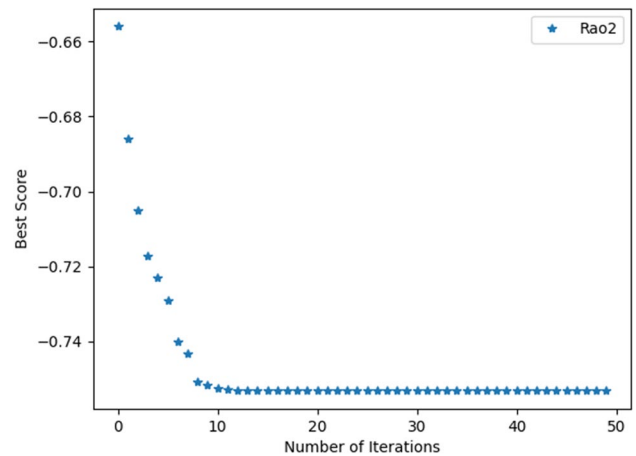**Fig. 16** Comparisons between GFRG based result and GRG

Fig. 18 Convergence curve for GFRG based Rao-2

$$Cs = 4.20238 \times A^{0.274019} \times B^{-0.287245} \\ \times C^{-0.0131667} \times D^{0.312621} \times E^{0.145953} \qquad (7)$$

$$KW = 0.226482 \times A^{0.00369101} \times B^{-0.022849} \\ \times C^{0.0100297} \times D^{0.0411395} \times E^{0.0100822} \qquad (8)$$
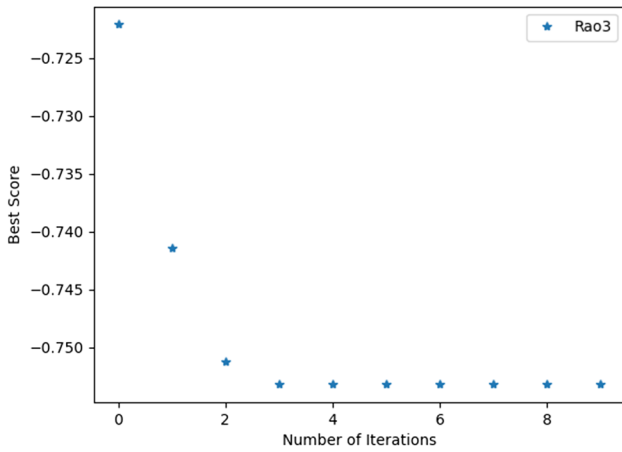
Fig. 19 Convergence curve for GFRG based Rao-3

$$RA = 4.02075 \times A^{0.0195866} \times B^{(-0.200821)}$$
$$\times C^{0.129639} \times D^{0.0898224} \times E^{0.12928} \tag{9}$$

$$GFRG = 0.8580 \times A^{(0.0595)} \times B^{(-0.1059)}$$
$$\times C^{(-0.0395)} \times D^{(0.0188)} \times E^{(-0.0585)} \tag{10}$$

The predicted global optimal parameter setting is obtained by maximizing GFRG through the Rao algorithms (Rao1, Rao2 and Rao3). The parameter setting appeared as $T_w = 16$N, $S_w = 3$ m/min, $P_f = 8$ kg/mm^2, $I_d = 21$ A, and $S_{on} = 14$ μs with the fitness function of 0.75318, shown in Table 8. Here, a fixed tuning setting (i.e., population size 30; iterations: 500) is used to obtain the solution. The optimal parameter setting obtained from the Rao algorithms has been compared against a number of well-known meta-heuristics algorithms (i.e., JAYA and I-GWO). The comparison results
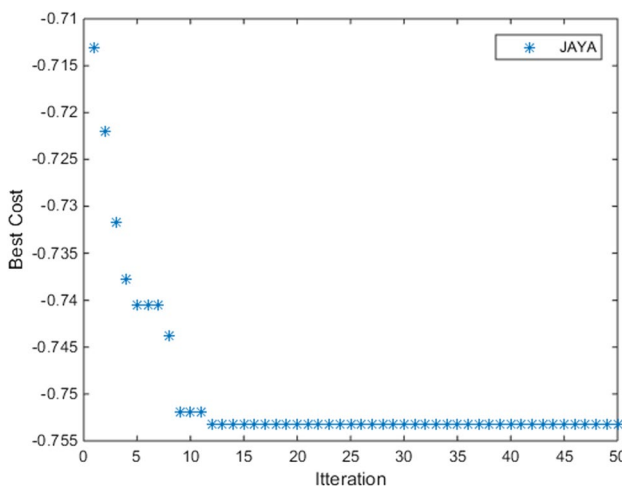

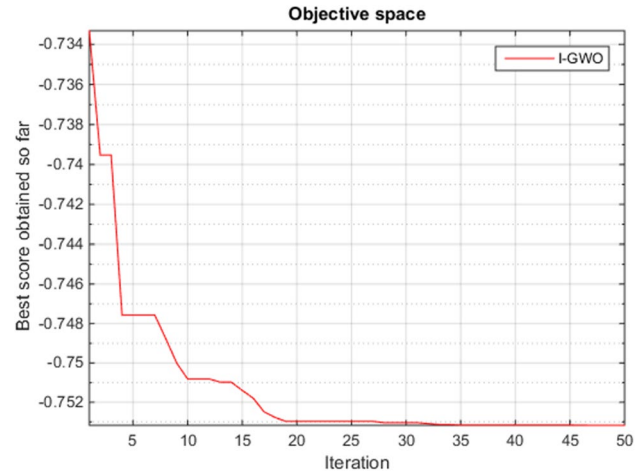**Fig. 20** Convergence curve for GFRG based JAYA

Fig. 21 Convergence curve for GFRG based Improved-Grey wolf optimizer (I-GWO)

notably recorded that the Rao1, Rao2 and Rao3 algorithms provide a global optimal solution in 0.685 s, 0.877 s and 0.524 s, respectively. On the other hand, the same parameter setting obtained from JAYA algorithm and I-GWO requires more time (i.e., 8.985 s and 12.550 s, respectively) with the same population size and iterations. The convergence plots with different algorithms have been shown in Fig. 22. The proposed hybrid optimization approaches not only obtained better outputs but also its run time is significantly minimized.

Confirmation Test

Tests of confirmation validate the optimality. Confirmatory tests are demeanours for validation and confirmation of the results. Table 5 reveals that experiment number 10 has obtained the highest overall assessment value. This means that the optimum input parameter setting of A2-B1-C2-D3-E1 (according to only GFRG) has the best multiple performance characteristics out of 27 experiments. The optimum parameter setting (A3-B1-C1-D3-E1) has been obtained by the GFRG-based Rao-Algorithms (see Table 8). The confirmatory test between the only GFRG-based setting and the GFRG-based Rao-Algorithms has been performed and is shown in Table 9. Overall machining improvement has been achieved by up to 4.10%. A similar type of confirmation test has been conducted by Shastri et al. [43].

Figure 23 shows the correlation between the experimental and optimized trial test results. The experiment has been conducted three times based on the optimal levels of input parameters obtained from GFRG based Rao-Algorithm. The average value is considered the final value and is shown in Table 9. The obtained optimum result has been compared with the GFRG result and exhibits an improvement

Table 8 Comparison of performance between Rao-1, Rao-2, Rao-3, Jaya and I-GWO algorithms

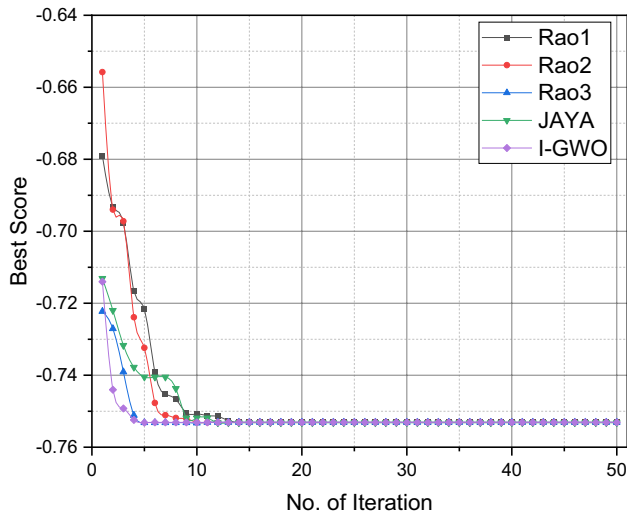| Algorithm	Optimal Parametric Combination					Fitness value	Computational Time (second)
	A [N]	B [m/min]	C [kg/mm²]	D [A]	E [μs]		
Rao-1	16	3	8	21	14	0.75318	0.685
Rao-2	16	3	8	21	14	0.75318	0.877
Rao-3	16	3	8	21	14	0.75318	0.524
JAYA	16	3	8	21	14	0.75318	5.985
I-GWO	16	3	8	21	14	0.75318	12.550

Fig. 22 Comparative study of different convergence plots for GFRG based optimization algorithm

of 9.55% in cutting speed, while 2.36% and 7.99% in KW and RA, respectively. Therefore, the GRFG-based Rao algorithm provides more accurate results (average improvement = 6.63%) compared to GFRG result. The improvement in Cs, KW, and RA has been shown in terms of the error bar in Fig. 23. The improvement may be due to changing levels of two essential parameters (i.e., higher level of T_w and low level of P_f). The higher value of T_w gives a strong force on the wire electrode, which provides wire stability during the machining. The stability of the wire provides better sparking phenomena in the working gap [36]. The lower level of P_f exerted a smaller force on the wire electrode that induced

lesser wire vibrations/deflections. Therefore, the debris produced during machining of Ti-3Al-2.5 V are conveniently removed from the cutting zone, and comparatively, a clean cut is obtained [31].

Comparison of this Work with the Existing Literature

In this section, the final results have been compared with the literature to fill the literature gap and identify the importance of the present study. Table 10 shows that the predicted optimum parameter setting obtained using GFRG based Rao-Algorithm is compared to the values obtained by the existing literature results. It is a much-expected result because the proper selection of machining parameters and hybrid multi-optimization technique proved the quality enhancement for Ti-3Al-2.5 V. Moreover, the advantage of "BroncoCut-X" also supports finding the best possible values of Cs, KW and RA variables together.

Conclusions

This study aimed to acquire experimental knowledge about the machining of Ti-3Al-2.5 V and consider the most important process variables such as T_w, S_w, P_f, I_d and S_{on}. The measurement machining characteristics are studied in terms of Cs, KW, and RA. The "BroncoCut-X" (Zinc-coated copper wire) was thoroughly tested under Taguchi's L_{27} array to achieve productivity with dimensional accuracy and surface quality. Lastly, a smart hybrid prediction tool has been performed for the machining outcomes. The work highlights the following conclusions from this investigation.

Table 9 Optimization results of GFRG based result versus GFRG- based Rao-Algorithms, JAYA and I-GWO

Method	A [N]	B [m/min]	C [kg/mm²]	D [A]	E [μs]	Cs (mm/min)	KW (mm)	RA (μm)	Overall (%)
Grey-Fuzzy (GFRG)	13	3	12	21	14	6.8	0.2330	4.13	
GFRG-based Rao-Algorithms, JAYA and I-GWO	16	3	8	21	14	7.45	0.2275	3.80	
Improvement (%)						9.55	2.36	7.99	6.63

Fig. 23 Comparison of experimental results (GFRG based result) and optimized trial test outcomes (GFRG Rao-Algorithm solutions)
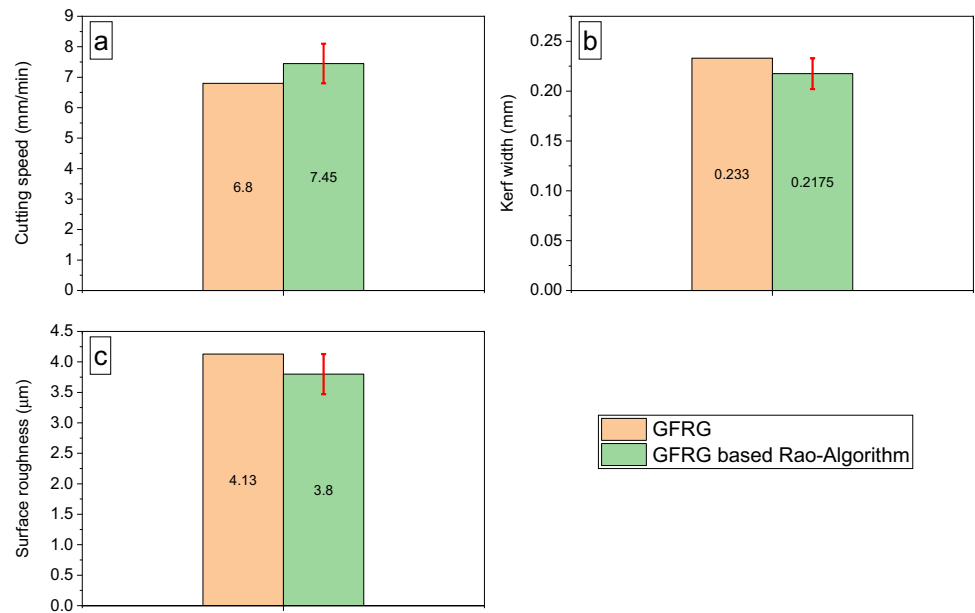

Table 10 The comparison present work with the existing literature

Investigator	Similarity			Differences		Responses		Improvement (%)
	Machining variables	Machining responses	wire electrode	Optimization technique	workpart and/or wire electrode	Existing Literature	Present work	
Zahoor et al. [24]	T_w, S_w, P_f, I_d, S_{on}	cutting speed	Broncocut-X (ϕ 0.20 mm)	Genetic algorithm	Inconel 718	3.998 mm/min	7.45 mm/min	46.33
Khan et al. [44]	S_{on}, S_w, T_w,		Broncocut-X (ϕ 0.20 mm)	×	Ti-6Al-4 V	3.4 mm/min		54.36
Kumar et al. [45]	S_{on}, I_d		×	Genetic algorithm	Nimonic-90; Zinc-coated brass wire (ϕ 0.25 mm)	1.84 mm/min		75.30
Banu et al., [46]	T_w, S_w,	kerf width	×	Taguchi method	stainless steel S304; Brass wire (ϕ 0.20 mm)	0.230 mm	0.2275 mm	1.1
Priyadarshini [47]	T_w, S_w, P_f, I_d, S_{on}		×	Taguchi method	AISI P20 tool steel; Zinc-coated brass wire (ϕ 0.20 mm)	0.2414 mm		6.11
Jadam [33]	T_w, S_w, P_f, I_d, S_{on}		×	×	Ti–6Al–4 V tool steel; Zinc-coated brass wire (ϕ 0.20 mm)	0.2796 mm		22.90
Ishfaq [48]	I_d, S_{on}	surface roughness	×	multi-objective genetic algorithm	Al6061-7.5% SiC; Brass wire (ϕ 0.25)	5.0 µm	3.80 µm	31.6
Patel et al. [49]	T_w, S_w, P_f, I_d, S_{on}		×	TOPSIS, MOORA, and GRA	Al6061; Brass wire (ϕ 0.25)	4.141 µm		8.97
Chopra et al. [50]	T_w, S_w, P_f, I_d, S_{on}		×	×	EN31 steel; Brass wire (ϕ 0.25)	5.234 µm		37.74

(×) objective not considered

1. The I_d has been the most contributing parameter for Cs during WEDM of Ti-3Al-2.5 V, having PCR of 34.91%. Whereas for KW and RA, P_f (having PCR 41.36%) and S_w (having PCR 34.15%) are the major contributing control variables, respectively

2. The surface morphology of the Ti-3Al-2.5 V WEDMed surface using "BroncoCut-X" has been characterized by the deposition of debris, melted materials, formation of pockmarks, craters, spherical droplets and micro cracks.

Moreover, the higher value of RA and crater size is due to increase I_d, which is validated through SEM micrograph.

3. From the SEM analysis of the recast layer, the "BroncoCut-X" confirms its excellent flushability characteristics. The observation showed that the recast layer varies in the range from 4.89 µm to 8.36 µm at 14 µs S_{on} and 2.02 µm to 8.84 µm at 21 µs S_{on}.

4. The obtained optimum parameter setting from GFRG-based Rao algorithms (Rao1, Rao2 and Rao3) has produced objective values in significantly shorter run-times compared to GFRG-based JAYA and GFRG-based I-GWO.

5. The optimal solution (obtained from GFRG base Rao-Algorithm) has been validated through confirmatory trials. The results depict high Cs of 7.45 mm/min. The minimum value of KW and RA obtained as 0.2275 mm and 3.80 μm, respectively.

6. A comparison study has been performed between the GFRG-based result and GFRG-based Rao Algorithm, and notable overall machining improvement by 6.63% and proved the goodness of the proposed hybrid multi-optimization technique.

The present work provided the best-performing optimal settings for the Ti-3Al-2.5 V under WEDM with the application of hybrid optimization approach. The presented hybrid optimization technique can be explored in other non-conventional machining such as ECM, EDM, and WJM and also in conventional machining like turning and drilling operations. Although, the present work only examined under the limited range of machining parameters of WEDM under the specific wire electrode, which could be considered a limitation. Future research could explore different combinations of parameters to further improve outcomes using the proposed hybrid optimization technique.

Data Availability Data will be made available on reasonable request.

Declarations

Conflict of Interest All authors confirm and declare no conflict of interest.

References

1. Javidrad F et al (2014) The MPAW of Ti-3Al-2.5V thin sheets and its effects on mechanical and microstructural properties. J Mater Eng Perform 23:666–672. https://doi.org/10.1007/s11665-013-0785-7

2. Mahapatra S et al (2007) Optimization of wire electrical discharge machining (WEDM) process parameters using Taguchi method. Int J Adv Manuf Technol 34:911–925. https://doi.org/10.1007/s00170-006-0672-6

3. Puri AB et al (2003) An analysis and optimisation of the geometrical inaccuracy due to wire lag phenomenon in WEDM. Int J Mach Tools Manuf 43:151–159. https://doi.org/10.1016/S0890-6955(02)00158-X

4. Sree Ram H et al (2022) Prediction of Kerf width and surface roughness of Al6351 based composite in wire-cut electric discharge machining using mathematical modelling. Materials 15:1102. https://doi.org/10.3390/ma15031102

5. Kuriakose S et al (2004) Characteristics of wire-electro discharge machined Ti6Al4V surface. Mater Lett 58:2231–2237. https://doi.org/10.1016/j.matlet.2004.01.037

6. Pasam VK et al (2010) Optimizing surface finish in WEDM using the Taguchi parameter design method. J Braz Soc Mech Sci Eng 32:107–113. https://doi.org/10.1590/S1678-58782010000200002

7. Devarajaiah D et al (2018) Evaluation of power consumption and MRR in WEDM of Ti–6Al–4V alloy and its simultaneous optimization for sustainable production. J Braz Soc Mech Sci Eng 40:400. https://doi.org/10.1007/s40430-018-1318-y

8. Gupta NK et al (2021) Revealing the WEDM process parameters for the machining of pure and heat-treated titanium (Ti-6Al-4V) alloy. Materials 14:2292. https://doi.org/10.3390/ma14092292

9. Sharma N et al (2021) Machining of Ti-6Al-4V biomedical alloy by WEDM: investigation and optimization of MRR and R using grey-harmony search. World J Eng ahead-of-print. https://doi.org/10.1108/WJE-05-2021-0278

10. Wang W et al (2020) Test method for residual stress analysis of the inner surface of small caliber Ti-3Al-2.5 V tubing by X-ray diffraction. Vacuum 177:109371. https://doi.org/10.1016/j.vacuum.2020.109371

11. Miller M et al (2015) Effect of heat treatments on the mechanical properties of Ti-3Al-2.5 V alloy. J Mater Eng Perform 24:3277–3290. https://doi.org/10.1007/s11665-015-1628-5

12. Babu N et al (2021) Experimental study on mechanical and tribological behaviour of Ti-3Al-2.5 V alloy at high load condition using response surface methodology. Adv Mater Process Technol: 1–14. https://doi.org/10.1080/2374068X.2021.1945259

13. Singh R et al (2020) Evaluating the sustainability pillars of energy and environment considering carbon emissions under machining ofTi-3Al-2.5 V. Sustain Energy Technol Assessments 42:100806. https://doi.org/10.1016/j.seta.2020.100806

14. Babu N et al (2020) Multi-response optimization of process parameters in wire electric discharge machining of Ti-3Al-2.5 V alloy using Taguchi integrated grey relational analysis. Int J Mech Prod Eng Res Dev 9:233–242

15. Ayesta I et al (2016) Influence of the WEDM process on the fatigue behavior of Inconel® 718. Int J Fatigue 92:220–233. https://doi.org/10.1016/j.ijfatigue.2016.07.011

16. Rehman M et al (2020) Parametric optimization in wire electric discharge machining of DC53 steel using gamma phase coated wire. J Mech Sci Technol 34:2767–2773. https://doi.org/10.1007/s12206-020-0609-2

17. Sharma P et al (2016) Effect of wire material on productivity and surface integrity of WEDM-processed Inconel 706 for aircraft application. J Mater Eng Perform 25:3672–3681. https://doi.org/10.1007/s11665-016-2216-z

18. Prohaszka J et al (1997) The effect of electrode material on machinability in wire electro-discharge machining. J Mater Process Technol 69:233–237. https://doi.org/10.1016/S0924-0136(97)00024-1

19. Reolon LW et al (2019) WEDM performance and surface integrity of Inconel alloy IN718 with coated and uncoated wires. Int J Adv Manuf Technol 100:1981–1991. https://doi.org/10.1007/s00170-018-2828-6

20. Lin B-T et al (2007) Using response surface methodology for optimizing deposited partially stabilized zirconia in plasma spraying. Appl Surf Sci 253:3254–3262. https://doi.org/10.1016/j.apsusc.2006.07.021

21. Kumar A et al (2022) Experimental investigation and optimization of machining performance characteristics during WEDM of inconel 718: On evaluation of wire electrodes and advanced parameter techniques. 236: 1645–1665. https://doi.org/10.1177/09544062211023115

22. Kumari C et al (2020) Experimental investigations and optimization of machining parameters for Magneto-rheological Abrasive Honing process. Mater Manuf Processes 35:1622–1630. https://doi.org/10.1080/10426914.2020.1779938

23. Mittal P et al (2020) Many-objective optimization of hot-rolling process of steel: A hybrid approach. Mater Manuf Processes 35:668–676. https://doi.org/10.1080/10426914.2019.1655157

24. Zahoor S et al (2021) WEDM of complex profile of IN718: multi-objective GA-based optimization of surface roughness, dimensional deviation, and cutting speed. Int J Adv Manuf Technol 114:2289–2307. https://doi.org/10.1007/s00170-021-06916-8

25. Varun A, Venkaiah N (2015) Simultaneous optimization of WEDM responses using grey relational analysis coupled with genetic algorithm while machining EN 353. Int J Adv Manuf Technol 76:675–690. https://doi.org/10.1007/s00170-014-6198-4

26. Wang T (1985) Grey functions and relational grade. Fuzzy Math 2:59–66

27. Lin C-T et al (2001) Improvement of machining accuracy by fuzzy logic at corner parts for wire-EDM. Fuzzy Sets Syst 122:499–511. https://doi.org/10.1016/S0165-0114(00)00034-8

28. Shabgard M et al (2013) Fuzzy approach to select machining parameters in electrical discharge machining (EDM) and ultrasonic-assisted EDM processes. J Manuf Syst 32:32–39. https://doi.org/10.1016/j.jmsy.2012.09.002

29. Sarkodie-Gyan T et al (2009) IEEE 529–534. https://doi.org/10.1109/ROBIO.2009.5420702

30. Rao R (2020) Rao algorithms: Three metaphor-less simple algorithms for solving optimization problems. 11:107–130. https://doi.org/10.5267/j.ijiec.2019.6.002

31. Ishfaq K et al (2021) Minimizing the corner errors (top and bottom) at optimized cutting rate and surface finish during WEDM of Al6061. Eng Sci Technol Int J 24:1027–1041. https://doi.org/10.1016/j.jestch.2021.01.008

32. Kumar A et al (2021) Experimental investigation and optimization of machining performance characteristics during WEDM of inconel 718: On evaluation of wire electrodes and advanced parameter techniques. Proc Inst Mech Eng C J Mech Eng Sci 236:1645–1665. https://doi.org/10.1177/09544062211023115

33. Jadam T et al (2019) Study of surface integrity and machining performance during main/rough cut and trim/finish cut mode of WEDM on Ti–6Al–4V: effects of wire material. J Braz Soc Mech Sci Eng 41:151. https://doi.org/10.1007/s40430-019-1656-4

34. Khan SA et al (2021) A detailed machinability assessment of DC53 steel for die and mold industry through wire electric discharge machining. Metals 11:816. https://doi.org/10.3390/met11050816

35. Naveed R et al (2019) Complex taper profile machining of WC-Co composite using wire electric discharge process: analysis of geometrical accuracy, cutting rate, and surface quality. Int J Adv Manuf Technol 105:411–423. https://doi.org/10.1007/s00170-019-04150-x

36. Selvakumar G et al (2020) Investigation on corner accuracy in wire cut EDM of AISI D3 tool steel. Int J Rapid Manuf 9:58–70. https://doi.org/10.1504/IJRAPIDM.2020.104426

37. Farooq MU et al (2020) Curved profiles machining of Ti6Al4V alloy through WEDM: investigations on geometrical errors. J Mater Res Technol 9:16186–16201. https://doi.org/10.1016/j.jmrt.2020.11.067

38. Nair H et al (2022) Experimental investigation on material removal rate, kerf width, surface roughness and the dimensional accuracy the accuracy of hole in Inconel 718 using wire electric discharge. Proc Inst Mech Eng Part E: J Process Mech Eng: 09544089221096025. https://doi.org/10.1177/09544089221096025

39. Rajmohan K et al (2017) Experimental investigation and prediction of optimum process parameters of micro-wire-cut EDM of 2205 DSS. Int J Adv Manuf Technol 93:187–201. https://doi.org/10.1007/s00170-016-8615-3

40. Pramanik A et al (2018) Processing of duplex stainless steel by WEDM. Mater Manuf Processes 33:1559–1567. https://doi.org/10.1080/10426914.2018.1453165

41. Somashekhar KP et al (2010) Material removal characteristics of microslot (kerf) geometry in μ-WEDM on aluminum. Int J Adv Manuf Technol 51:611–626. https://doi.org/10.1007/s00170-010-2645-z

42. Mirjalili S et al (2014) Grey wolf optimizer. Adv Eng Softw 69:46–61. https://doi.org/10.1016/j.advengsoft.2013.12.007

43. Shastri RK et al (2021) Sustainable electrical discharge machining of Nimonic C263 superalloy. Arab J Sci Eng 46:7273–7293. https://doi.org/10.1007/s13369-020-05211-0

44. Khan SA et al (2021) Exploring the feasibility of novel coated wires in wire EDM of Ti-6Al-4 V aerospace alloy: a case of multi-pass strategy. J Braz Soc Mech Sci Eng 43:273. https://doi.org/10.1007/s40430-021-02994-7

45. Kumar V et al (2017) WEDM of nickel based aerospace alloy: optimization of process parameters and modelling. Int J Interactive Des Manuf (IJIDeM) 11:917–929. https://doi.org/10.1007/s12008-016-0298-3

46. Banu A et al (2017) Analysis of WEDM process parameters on surface roughness and Kerf using Taguchi method. Int J Eng Mater Manuf 2:103–109. https://doi.org/10.26776/ijemm.02.04.2017.04

47. Priyadarshini M et al (2019) Machining of sub-cooled low carbon tool steel by wire-EDM. Mater Manuf Processes 34:1316–1325. https://doi.org/10.1080/10426914.2019.1662035

48. Ishfaq K et al (2020) Optimization of WEDM for precise machining of novel developed Al6061-7.5% SiC squeeze-casted composite. Int J Adv Manuf Technol 111:2031–2049. https://doi.org/10.1007/s00170-020-06218-5

49. Patel JD et al (2019) WEDM process parameter selection using preference ranking method: a comparative study. Int J Manuf Res 14:118–144. https://doi.org/10.1504/IJMR.2019.099978

50. Chopra K et al (2019) Detailed Experimental Investigations on Machinability of EN31 Steel by WEDM. Trans Indian Inst Met 72:919–927. https://doi.org/10.1007/s12666-018-1552-0